Study of Interfacial Mass Transfer on Vapor Bubbles in Microgravity

G. Picker

EADS Space Transportation, Payloads / Fluid Physics
D-88039 Friedrichshafen, Germany
phone: +49 754584279, Fax: +49 754584429
Email: gerold.picker@space.eads.net

J. Straub

Institute for Thermodynamics, Technical University Munich
D-85748 Garching, Germany
Phone: +49 8928916234, Fax: +49 8928916218
Email: straub@td.mw.tum.de

Abstract

The knowledge of interfacial heat and mass transfer is important for environmental and technical applications, especially nowadays for numerical simulations of two phase problems. However, the data available up to now are inconsistent, because most experiments performed on earth suffer under buoyancy and convection, and thus the boundary conditions at the evaluation could not clearly be defined. Therefore, we seized the opportunity to investigate interfacial heat and mass transfer in microgravity environment. In these experiments the growth and collapse in the overall superheated and subcooled bubles, respectively, liquid or free vapor bubbles were observed at various liquid temperature and pressure states and over periods of from a few seconds up to 300 seconds. It was for the first time that such very long periods of bubble growth could be observed. The experimental set-up allowed the control of the liquid supersaturation before the bubbles were initiated by a short heat pulse at a miniaturized heater. Therefore it was possible to perform a systematic parametric study. The measured curves for vapor bubble growth are in good agreement with our numerical simulation. Based on this model the kinetic coefficients for the evaporation and condensation according to Hertz-Knudsen have been derived from the experimental data.

Keywords: Nucleation, bubble dynamics, interfacial phenomena, evaporation and condensation kinetics, microgravity

1. Introduction

The evaporation and condensation process is very important for environmental processes such as the evaporation on free surfaces of lakes, seas and rivers, the formation of clouds, and generally for meteorology. Likewise it is very important for many technical applications in the heat transfer of two phase problems as in chemical engineering, power conversion, heating and cooling systems. In particular the heat transfer in boiling and condensation is strongly influenced by the evaporation and condensation process. In this paper our research is focused on vapor bubble growth and vapor bubble collapse in a supersaturated and subcooled liquid, respectively. To overcome the problems of former experimental works (Dergarabedian, 1953; and Cole, 1966),

such as short observation time and non-uniform temperature fields around the bubbles, the experiments were performed under microgravity conditions. We were able to use the German drop tower at ZARM in Bremen, the Japanese drop shaft, JAMIC in Hokkaido, and Space-Lab-Missions such as IML2 (1994) and LMS (1996). During the Space-Shuttle-Missions the experiments were performed in the BDPU (Bubble, Drop and Particle Unit), ESA's multi-user facility developed for fluid physics experiments.

2. Bubble Growth and Collapse

2.1 The thermodynamic process

Differing from most other investigations to study the kinetics of phase transition, in this case

the experiments are performed in a liquid which was transferred entirely into a supersaturated metastable state by pressure reduction below the saturation pressure of the liquid. During this process the whole liquid could be maintained at a nearly isothermal and uniform temperature, apart from small temperature change due to the isentropic pressure change. The thermodynamic process is sketched on a basic p,T - phase diagram of a fluid, shown in *Figure 1*. For safety reasons, as pressure limitation, convenient temperature range, non-toxicity, we used as test fluids R11 and R113. The pure and degassed liquid was heated to a constant temperature T_1 which was maintained by temperature control.

By increasing the pressure above saturation to p1 (*Figure 1*, state 1), vapor nuclei on the surface of the cell walls are inactivated down to a distinct size given by

$$R_n = \frac{2\sigma}{\Delta p} = \frac{2\sigma}{p_1 - p_2} \qquad (1)$$

The isothermal supersaturated liquid is achieved by reducing the pressure of the liquid from the pressure p1 to p3 below the saturation pressure $p2 = psat$, corresponding to the liquid temperature. In this metastable, supersaturated state vapor bubbles are generated by a short heating pulse of a thermistor used as a miniaturized heater with a diameter of about 250 µm. The nucleation process is assumed to be isothermal according to the nucleation theory (path 1, *Figure 2a*), the radius of the activated bubbles is equal to a critical radius, which can be estimated with equation (1) inserting the pressure difference (p2 − p3). In the following phase (path 2, *Figure 2a*) the bubble growth is controlled by the increasing temperature difference (Tl -Tsat.) along the vapor pressure line, where the saturation pressure decreases with increasing bubble radius. This period is widely referenced in the literature (van Stralen, 1979) as hydrodynamic bubble growth, even if it is governed by the decreasing temperature difference. But even in this state at the end of path 2, at point 4 in *Figure1*, where p3 = p4, the bubble is still so small that it can hardly be observed.

Now we may assume that in the bubble the pressure is nearly at saturation according to the liquid pressure psat ≈ p3 (indeed it is a little higher according to the small radius of the bubble, equation (1)), and we assume the phase boundary temperature follows the saturation pressure. Now the further bubble growth is governed by unsteady heat conduction in the liquid, due to the potential difference ΔTsat between the liquid bulk temperature and the temperature at the phase interface (*Figure 2b*). This temperature difference guarantees the transport of the latent heat to the bubble, necessary for the evaporation.

For this simplified description of the process, the temperature difference at the phase interface according to the kinetic theory is neglected. During the subsequent bubble growth, the system pressure is kept nearly constant by means of a metal bellows and a counter pressure provided by pressurized nitrogen gas from a pressure vessel and a pressure control system.
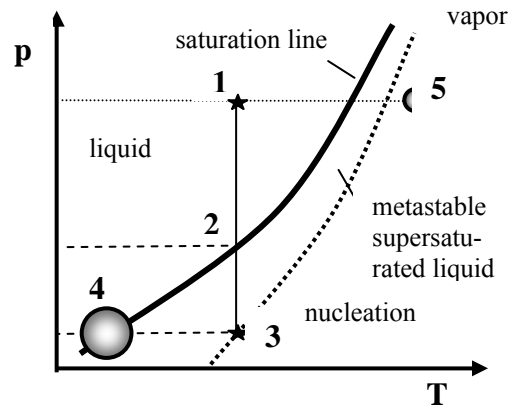
Figure 1. Sketch of the thermodynamic process on a p,T -phase diagram
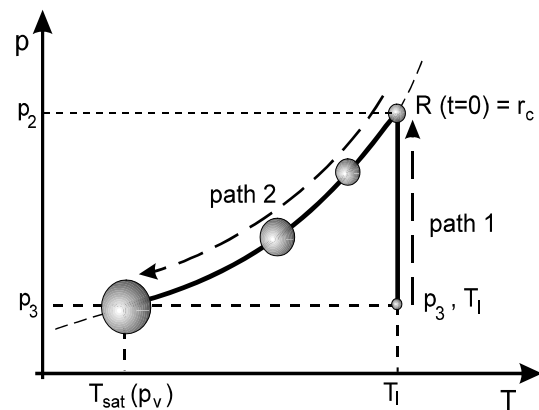
Figure 2a. Bubble Growth on the p, T phase diagram
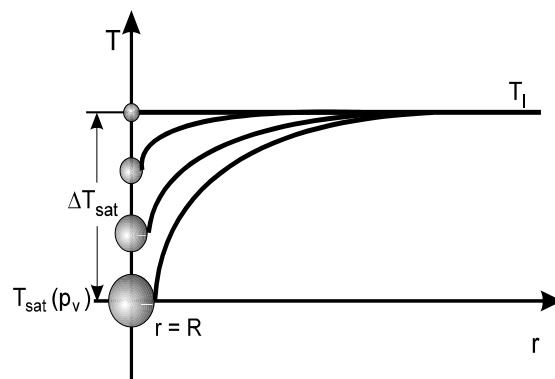
Figure 2b. Temperature field around the bubble

If the bubble was grown up to a certain size the growth was stopped by increasing the pressure in the liquid cell to the initial one by means of the pressurized nitrogen and the bellows, in *Figure 1* from point 4 to 5. The vapor in the bubble is compressed, and depending on the speed of this process the vapor inside can be superheated, or at a slow compression process it may follow nearly the saturation line up to the saturation temperature of p1. The liquid phase is compressed too, but from point 3 to point 1 with only a very small increase of the temperature. Finally the bubble condensation and collapse is caused by the large temperature difference between T_5 and T_1 respectively, and a temperature between T_4 and T_1 because the liquid boundary layer was previously cooled during evaporation process before.

For this research microgravity conditions are necessary to produce and to observe large bubbles, which are not driven by buoyancy forces from the location of nucleation. Furthermore, the temperature field around the bubbles is not disturbed by buoyancy-induced convection. Thus the boundary conditions can be defined and the experimental results can be compared with an idealized theoretical formulation of the problem.

2.2 Numerical formulation of bubble growth and collapse

The formulation of the problem is similar to that one suggested by Beylich (1983) and it is adjusted to the existing problem by Picker (1998). A spherical bubble, which grows in a quiescent liquid with initial uniform temperature distribution is assumed to be of infinite extent. Thus the radial-coordinate r and the time t are the only independent variables. The conservation equations for this problem, for the liquid and vapor phase, are as follows.

2.2.1 Equation of Continuity for the liquid

Assuming that the density in the bulk liquid ρ_l outside the bubble is constant, the equation of continuity can be integrated and the result is given by equation (2)

$$v_l(r,t) = \frac{1}{r^2} R(t)^2 w_l(t) \qquad (2)$$

where r is the radial coordinate of the system originating in the bubble center and $v_l(r,t)$ is the velocity of displacement of the liquid caused by the movement of the bubble surface due to bubble growth with the velocity $w_l(t)$.

2.2.2 Equation of Motion for the Liquid

The basic momentum equation can be integrated under the assumption of constant density

ρ_l, if all volumetric forces like gravity g are neglected:

$$p(r,t) - p(r=\infty,t) = \rho_l \left(\frac{2R\ \dot{R}\ w_l + R^2 \dot{w}_l}{r} - \frac{1}{2} \frac{R^4 w_l^2}{r^4} \right) (3)$$

The liquid velocity $v_l(r=\infty,t)$ far from the bubble is considered to vanish.

2.2.3 Equation of the thermal energy flow in the liquid

For this problem with spherical symmetry, the conservation equation for internal energy reduces to the equation of thermal energy flow in the liquid such that

$$\frac{\partial T_l}{\partial t} + v_l \frac{\partial T_l}{\partial r} = \frac{4}{3} \frac{\mu_l}{\rho_l c_l} \left(\frac{\partial\ v_l}{\partial\ r} - \frac{v_l}{r} \right)^2 \qquad (4)$$
$$+ \frac{\lambda_l}{\rho_l c_l} \frac{1}{r^2} \frac{\partial}{\partial r} \left(r^2 \frac{\partial T_l}{\partial r} \right)$$

if the common simplification for the internal energy $U = c_l\, T_l$ is applied and the thermal conductivity λl and the specific heat cl are set constant.

2.2.4 Equation of Continuity for the Vapor

The equations for the interior of the vapor bubble are given briefly below. Inside the vapor bubble the density ρ_v, the thermal conductivity λ_v and the specific heat c_v are considered to be functions of the vapor temperature $T_v(r,t)$.

$$\frac{\partial \rho_v}{\partial t} + \frac{\partial}{\partial r}(\rho_v v_v) + \frac{2}{r} \rho_v v_v = 0 \qquad (5)$$

2.2.5 Equation of motion for the vapor

$$\frac{\partial v_v}{\partial t} + v_v \frac{\partial v_v}{\partial r} = -\frac{1}{\rho_v} \frac{\partial\ p_v}{\partial\ r} \frac{4}{3} \frac{\mu_v}{\rho_v} \frac{\partial}{\partial\ r} \left(\frac{\partial\ v_v}{\partial\ r} \frac{2v_v}{r} \right) \ (6)$$

2.2.6 Equation of the thermal energy flow for the vapor

$$\rho_v \left(\frac{\partial U_v}{\partial t} + v_v \frac{\partial U_v}{\partial r} \right) = -p_v \left(\frac{\partial v_v}{\partial r} + \frac{2v_v}{r} \right) \qquad (7)$$
$$+ \frac{4}{3} \mu_v \left(\frac{\partial v_v}{\partial r} - \frac{v_v}{r} \right)^2 + \frac{1}{r^2} \frac{\partial}{\partial r} \left(\lambda_v r^2 \frac{\partial T_v}{\partial r} \right)$$

where ideal gas is assumed for equations of state: $Uv = cv(Tv)\, Tv$, and $pv = \rho v\, k/m\, Tv$.

2.2.7 Boundary and Coupling Conditions of Conservation Equations

The conservation equations for the liquid outside and the vapor inside the bubble are coupled at the bubble surface. On the vapor and liquid side of the bubble surface (*r=R*), different velocities $v_v(r=R)=w_v$ and $v_l(r=R)=w_l$ are used for mass conservation such that

$$\rho_1(v_1 - \dot{R}) = \rho_v(v_v - \dot{R}) = -\dot{m} \quad r=R \quad (8)$$

over the interface.

The momentum equation for the interface

$$p_1 + \frac{2\sigma}{r} = p_v + \rho_v\left(v_v - \dot{R}\right)\left(v_v - v_1\right) +$$
$$\frac{4}{3}\mu_l\left(\frac{\partial\ v_l}{\partial\ r} - \frac{v_l}{r}\right) - \frac{4}{3}\mu_v\left(\frac{\partial\ v_v}{\partial\ r} - \frac{v_v}{r}\right) \quad (9)$$

introduces the surface tension σ and the dynamic viscosity μ_v and μ_l of both phases. equation (9) follows results found by Hsieh (1965) transferred to spherical symmetry coordinates. Beylich (1985) explained the derivation from Hsieh (1965) in detail by analyzing the coupling of continuum and molecular-kinetic momentums at the interface of the 2-phase system. The balance considers the momentum exchange between vapor at velocity w_v and liquid velocity w_l at an interface moving at velocity $\dot{R}$. By comparison of the characteristic scales for the terms in equation (9) it was found that viscous terms are significant for the beginning of the hydrodynamic bubble growth (path 2, *Figure 2a*).

The energy equation for the interface describes the balance between the latent heat of evaporation h_{lv} necessary for the mass flow $\dot{m}^*$ per surface unit and the heat conduction in the liquid as well as in the vapor:

$$\lambda_l\frac{\partial\ T_l}{\partial\ r} - \lambda_v\frac{\partial\ T_v}{\partial\ r} = \dot{m}^*\left[h_{lv} + \frac{4}{3}\frac{\mu_l}{\rho_l}\left(\frac{\partial\ v_l}{\partial\ r} - \frac{v_l}{r}\right) - \right.$$
$$\left. \frac{4}{3}\frac{\mu_v}{\rho_v}\left(\frac{\partial\ v_v}{\partial\ r} - \frac{v_v}{r}\right) - \frac{1}{2}(\dot{R} - v_l)^2 + \frac{1}{2}(\dot{R} - v_v)^2\right] \quad (10)$$

The heat available for the evaporation can be calculated with the liquid temperature gradients at the phase interface.

A further boundary condition is the temperature gradient at the center expressed as

$$\left(\frac{\partial\ T}{\partial\ r}\right)_{r=0} = 0 \quad (11)$$

The boundary condition for the liquid at $r\rightarrow\infty$ is the initial temperature of the liquid, given by

$$T(r \rightarrow \infty, t) = T_l \quad (12)$$

This boundary condition is justified because the bubble and the boundary layer are small compared to the size of the test cell or the computational domain.

2.2.8 Kinetic theory for interfacial mass transfer

The calculation of the mass flow rate over the liquid vapor interface can be derived from the kinetic theory according to Hertz (1882), Knudsen (1909) and Schrage (1953) . Kinetic theory

allows a straight forward derivation for the condensing mass flow. A dynamic equilibrium of condensing and evaporation flows at the interface leads to a similar expression for the evaporation flux. Further details of this theory will not be explained here.

For the case of near equilibrium, the net mass flow over a liquid vapor interface is the difference between the evaporating and condensing molecular mass flows. According to the temperature relation at the phase interface, either evaporation or condensation is dominant. The net mass flow over the liquid vapor interface is given by:

$$\dot{m}^*_{netto} = \sqrt{\frac{k}{2\pi m^*}}\left[(\rho_v(T_{Wv})\sqrt{T_{Wv}} - \rho_v(T_{Wl})\sqrt{T_{Wl}})\right] \quad (13)$$

Many researchers (reviewed in Paul, 1962 and Pound, 1972) tried to verify this theory by using different measurement techniques. In most measurements the mass flow rate predicted by the theory was not reached in the experiment. The evaporation and condensation coefficients β_e and β_c representing the ratio of experimental mass flow rate to theoretical mass flow rate, were introduced. The values of the coefficients have varied over decades, see Marek and Straub (2001). Introducing the coefficients and treating the vapor as ideal gas results in

$$\dot{m}^*_{netto} = \sqrt{\frac{m^*}{2\pi k}}\left(\beta_e\frac{p_{sat}(T_{Wl})}{\sqrt{T_{Wl}}} - \beta_c\frac{p_v}{\sqrt{T_{Wv}}}\right) \quad (14)$$

which represents a realistic equation describing the interfacial mass flow during bubble growth and condensation according to the kinetic theory. This mass flow must be equal to the one in equation (10).Hence equation (14) is used for the numerical model.

2.2.9 Handling of the Numerical Model

Without further presentation of details the set of equations (2)-(7), (8)-(12), (14) describing the problem was simplified according to Beylich (1985) and solved simultaneously for both domains inside and outside the bubble surface. The energy equations, equations (4), (7) were discretized using a finite difference scheme, with a non-equidistant grid spacing Δr. The grid is stretched with increasing distance from the bubble surface. In this case the steep temperature gradient in the vicinity of the bubble can be treated sufficiently. Equations. (1) and (11)-(12) were used together with a time dependent pressure profile (see *Figure 4*) as boundary and initial condition for the numerical integration. The complete system of equations was integrated using a fourth order Runge-Kutta algorithm with an adaptive step-size control. The main product

of a simulation run is a R-t curve related to a set of physical parameters for a specific bubble growth and condensation process, see *Figure 6*. Further details of the numerical model are described in Picker (1998).

3. Experiments

3.1 Experiments on IML 2

During the IML 2 Spacelab mission (1994) this experiment was conducted in the ESA multi-user facility BDPU (Bubble, Drop and Particle Unit). A special Test Container was designed for our experiment, using standard interfaces of the facility for power supply, experiment control and data acquisition as well as the optical observation of the facility. This was the first time that undisturbed bubble growth could be observed over a very long time, up to 300 seconds.

Due to the extended microgravity time more than 30 independent experiment runs were carried out using FREON 11 as a model fluid. During the preparations of the Spacelab mission we had the chance to perform several experiments in the Japanese drop shaft JAMIC. A large number of experiment runs were conducted in the ZARM drop (1992/93) tower in Bremen. The principle of free fall is used for the compensation of the earth gravity in order to achieve a microgravity environment for the experiment. The height of the evacuated drop tube in the tower is about 110 m, which results in a free fall time of 4.7 seconds.

3.2 Experimental hardware

The principle for the various experimental set-ups was the same. In the following only the BDPU and test container set-up used for the IML-2 mission will be explained.

The BDPU is ESA's multi-user facility for fluid physics experiments for the Spacelab. The flexibility of this facility is ensured in that way, that for various experiments specific test containers are designed. The BDPU provides the power supply, the various optical observation methods and the data interface to the Spacelab/Shuttle system. Each observation path is recorded by a video camera or an extra 16 mm film camera. The experiment is executed by a specific software, which controls all systems of the facility and the test-container. From the ground center at the Marshall Space Flight Center in Huntsville Alabama the principal investigator's team could observe the experimental runs during the mission in real time video and all important experimental data were immediately available. By telecommanding from the ground the essential experimental parameters were adjusted depending on the observed data.

The experiment specific hardware (*Figure 3*), designed by DASA/Dornier, Germany, was squeezed into a small containment of 45x15x30 cm³. The liquid cell itself in the center of the container was in principle spherical with a diameter of 55 mm. It had four windows of sapphire with an optical diameter of 40 mm for two perpendicular observation directions. The fluid and cell were isothermally controlled in a range from 20 to 90 °C. The liquid pressure was controlled by means of a combined electronic and mechanical system from 1 to 7 bar with an accuracy of 2 mbar. Eight identical thermistors were directly placed in the liquid to measure the liquid temperature around the growing bubbles.

The experiments were performed at six different fluid temperatures (30, 40, 50, 60, 70, 85 °C). At each temperature three to seven experimental runs at various isothermal supersaturation pressures ranging from 50 to 300 mbar were achieved, resulting in a total number of 32 experiment cycles.

3.3 Evaluation

Using digital image analyses the video images and 16 mm films were post-processed to measure radius-time-curves (R-t-curves). These curves were in good agreement with the simplified approximate solutions for the bubble growth suggested by several authors (e.g. Forster and Zuber, 1954; Plesset and Zwick, 1954; Scriven, 1959), who characterized the experimental condition with the Jakob number.

$$Ja = \frac{(T_\infty - T_{sat}(p_\infty))\rho_l c_l}{\rho_v h_{lv}} \qquad (15)$$

The Jakob number describes the ratio between the sensible heat due to the temperature difference $\Delta T_{sat} = T_\infty - T_{sat}(p_\infty)$ in the liquid and the latent heat of evaporation.

Since the simplified approximations are insufficient to study the heat and mass transfer at the interface of a vapor bubble in detail, the numerical model described in section 2.2 was used to evaluate the measured R-t-data.
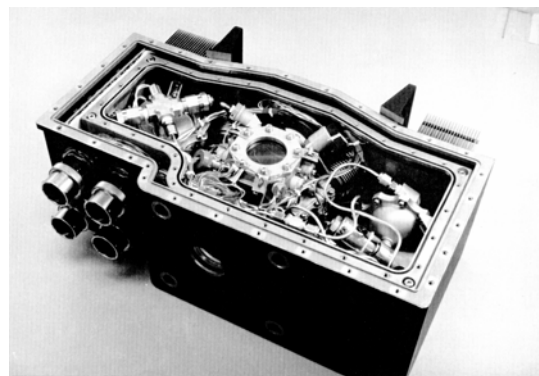
Figure 3. BDPU TC3: Experimental equipment for bubble growth and condensation study on board Spacelab
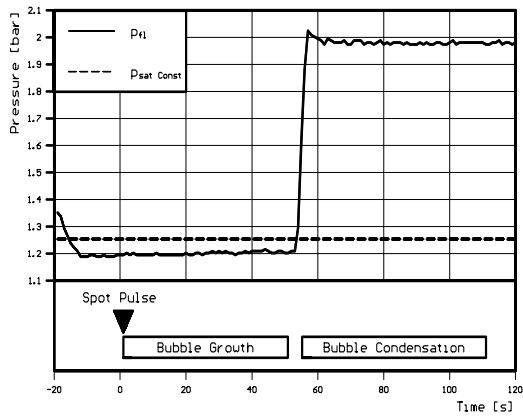
Figure 4.Typical pressure time diagram of one experiment run (T_l = 29.7 °C, IML-2/exp. 14), see Figure 5
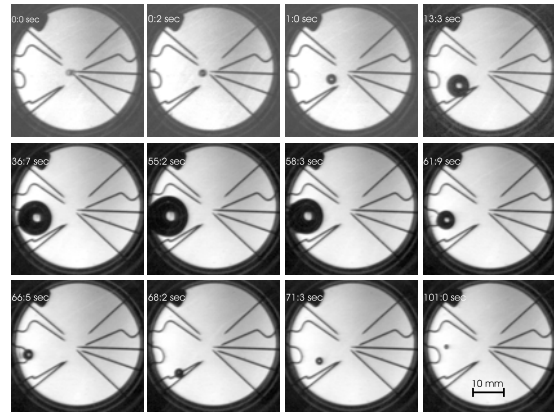
Figure 5. Growing and shrinking vapor bubble under μg,
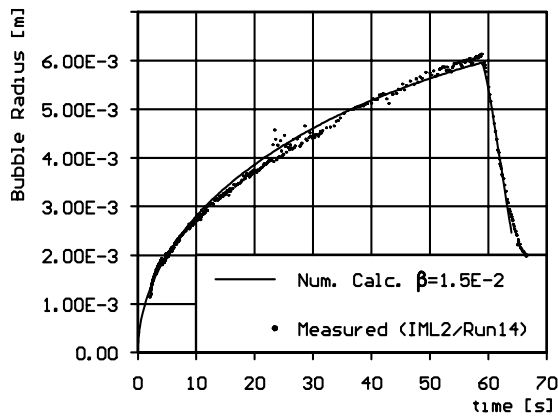
Figure 6. Measured and calculated R,t curves (bubble from Fig. 5) T_l = 29.7 °C, Δp_{sat} = 60 / 650 mbar, (IML-2)
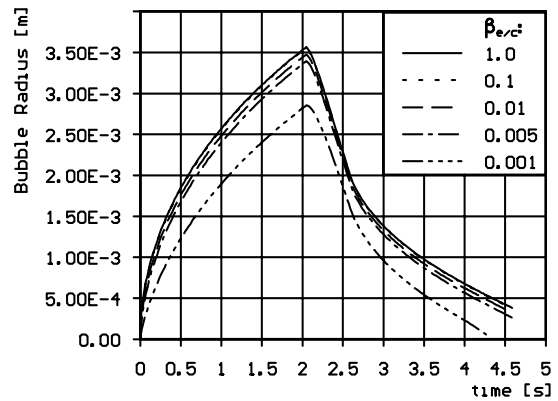
Figure 7. Influence of the evaporation-condensation coefficients $\beta e/c$ on the R-t-curve (R11, Tl =35.1 °C, $\Delta psat$ = 200mbar, Ja = 2.3)
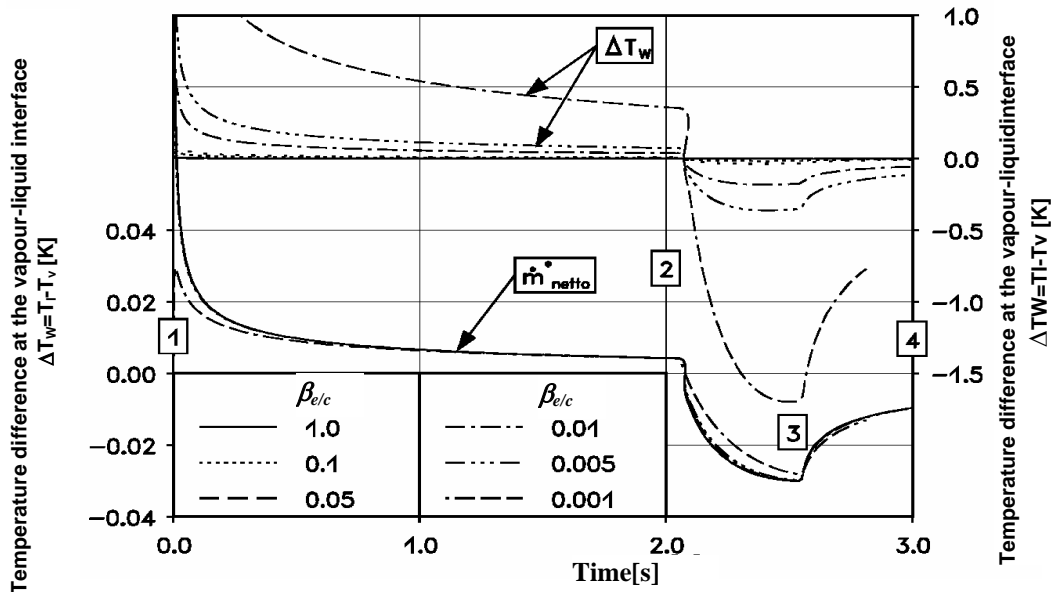
Figure 8. Influence of the evaporation-condensation coefficients $\beta_{e/c}$ on the temperature difference at the interface (R11, T_l =35.1 °C, Δp_{sat} = 200mbar, Ja = 2.3)
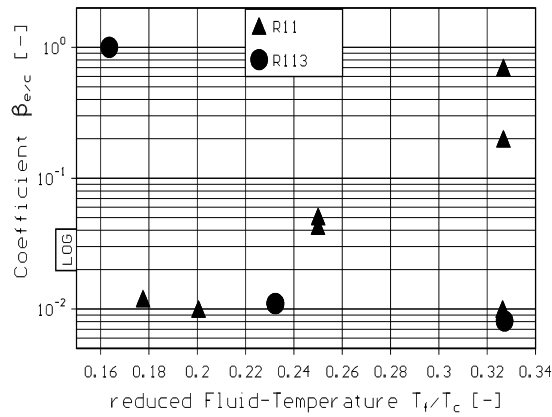
Figure 9. Evaporation coefficients as a function of the reduced liquid temperature

It was assumed here that evaporation and condensation coefficients have the same values ($\beta_e = \beta_c$), which was identified to be a valid assumption for the case of bubble growth and condensation(Picker,1998). For the calculation of the evaporation and condensation coefficient the liquid temperature at the phase interface would be necessary, which could not be measured directly. So the described numerical model is used to determine this coefficient. The measured R-t curve is quantitatively compared to the numerical R-t data, based on the measured experimental boundary conditions. Both coefficients are adapted successively, using a optimization method until the difference between the measured and calculated R-t curves is minimized.

4 Results of the Experiments

4.1 Bubble growth

Figure 4 displays a typical pressure sequence measured for the vapor bubble growing and shrinking as given in *Figure 5*. The bubble growth was initiated by a pulse of a spot heater at which a small bubble at the beginning can be seen. The movement of the bubble during growth maybe caused by the momentum at bubble detachment, by the liquid replacement and a flow caused by the replaced liquid to the bellows. *Figure 6* displays the measured radius time curve for this bubble growth. The fluid temperature was 29.7 °C with a supersaturation of approximately 60 mbar, that equals an isobaric ΔT_{sat} of 1.4 K and a Jakob number of Ja = 1.5. The numerical radius time curve of the bubble shown in *Figure 6* was calculated considering the additional heat produced by the short heat pulse from the spot heater. An evaporation-condensation coefficient of $\beta_{e/c}$=0.015 was found to represent the measured data with the smallest deviation.

4.2 Kinetic Coefficients

The liquid temperature at the phase interface was calculated with the numerical model. The temperature at the vapor side of the interface was assumed equal to the saturation temperature corresponding to the pressure p_v inside the bubble. The influence of the evaporation and condensation coefficient on the growth and condensation of a vapor bubble is shown in *Figure 7*. The corresponding net mass flow over interface and temperature difference at the vapor liquid interface according to equation (14) is displayed in *Figure 8*.

For low Jakob numbers, values of β_e, $\beta_c <$ $1 \cdot 10^{-1}$ have a significant influence on the bubble dynamics. For the conditions studied here only coefficients smaller than this limit result in significant non-equilibrium at the interface, which leads to a detectable limitation of the interfacial mass flow rate. A summary of the coefficients obtained from the pre- and IML2-experiments is given in *Figure 9*. The coefficients are the best representation of the measured data curves.

Based on the numerical model it was also investigated if a different evaporation and condensation coefficient would give reasonable radius-time curves for the bubble growth and condensation. For significantly modified values $\beta e \neq \beta c$ the bubble either could not grow from its nucleation radius ($\beta e << \beta c$) or resulted in an extremely high growth rates ($\beta e >> \beta c$), which were not representative for the experimental findings. A variation of the ratio $\Delta\beta = (\beta e - \beta c)/\beta e$ in the range +5% to -5% revealed still a very significant influence on the radius-time curve. From this results it was concluded that any difference of the coefficients above $|\Delta\beta| > 1\%$ gives unrealistic bubble growth and condensation rates for the investigated experimental situation. Therefore the assumption that evaporation and condensation coefficient has the same values ($\beta e = \beta c$) could be confirmed for the experimental conditions investigated here. This can also be explained by the derivation of equation (14), which assumed a balanced dynamic equilibrium at the interface, requiring $\beta e = \beta c$ for $\dot{m}^*_{netto} = 0$.

For R113, we found decreasing coefficients $\beta_{e/c}$ with increasing fluid temperature. The evaporation and the condensation coefficients range from 1.0 at 35 °C down to $8.1 \cdot 10^{-3}$ at 70 °C.

In the case of R11, coefficients in the range of 0.7 to $1 \cdot 10^{-2}$ were obtained without observing a specific dependence on the fluid temperature. The main reason for the scattered results with respect to fluid temperature for R11 was found to be the contamination with solved air. R11 has a strong tendency to solve N_2, O_2 and CO_2, which could not be removed completely by our exten-

sive degassing. Several measurements of the equilibrium saturation pressure confirmed this, but were evaluated, after the measurement campaigns for the bubble growth experiments had already been finished. R113 was found to be much less sensitive to this behavior. The contamination with surrounding gas was a particular problem for the Spacelab experiment. The experimental hardware had to be delivered completely filled with experimental fluid three months in advance to the mission. Minimum leakage and diffusion through the O-ring seals of the fluid cell increased the concentration of N_2 during this storage period for the bubble growth experiments onboard of Spacelab. For future experiments more efforts should be taken to detect and avoid this fluid contamination.

5 Conclusions

Systematic experimental series provided data about the growth and shrinkage of free vapor bubbles in a homogenous supersaturated and subcooled liquid under microgravity. The growth and collapse of these bubbles were observed up to 300 seconds. The bubble growth rates in R11 and R113 were determined at various liquid temperature levels and supersaturation values. The measured curves for vapor bubble growth are in excellent agreement with our numerical simulation. With the same model the experimental values of the bubble growth curve, the temperature at the bubble interface is calculated. With this temperature and the temperature inside the bubble the mass flow through the liquid vapor interface and subsequently the evaporation and the condensation coefficients were determined. Contamination with solved gases had significant influence on the observed kinetic coefficients especially for R11.

Nomenclature

a   Thermal diffusivity
A   surface
c   specific heats
h   specific enthalpy
Ja   Jakob number

k   Boltzmann constant
m   mass
m*   molecular mass
$\dot{m}^*$ mass flow per unit of the surface
p   pressure
r   radial coordinate
R   bubble radius
t   time
T   temperature
U   internal energy
v   velocity
w   velocity at the interface

Greek Symbols

β   evaporation and condensation coefficient
λ   thermal conductivity
μ   dynamic viscosity
ρ   density
σ   surface tension

Subscripts

c   condensation
e   evaporation
l   liquid
sat   saturation
v   vapor
w   condition at the interface
∞   condition in the liquid far away from interface

References

Beylich, A. E., 1985, Dynamik und Thermodynamik sphärischer Dampfblasen, *VDI Forschungheft*, vol. 630, pp. 1-27.

Cole, R., and Shulman, H. L.,1966, Bubble Growth Rates at High Jakob Numbers, *Int. J. Heat and Mass Transfer*, vol. 9, pp. 1377-1390.

Dergarabedian, P., 1953, The Rate of Growth of Vapor Bubbles in Superheated Water, *J. of Appl. Mech.*, vol. 20, pp. 537 - 545.

Forster, H. K, and Zuber, N.,1954, Growth of a Vapor Bubble in Superheated Liquid, *J. of Appl. Phys.,* vol. 25, pp. 493-500.

Hertz, H., 1882, *Ann. Phys.*, 17, p. 193.

Hsieh, D., 1965, Some Analytical Aspects of Bubble Dynamics, *J. of Basic Eng., Transactions of the ASME*, pp. 991-1005.

Knudsen, M., 1909, *Ann. Phys.*, 29, p. 179.

Marek, R. and Straub, J. 2001, Analysis of the Evaporation and the Condensation Coefficient of Water, *Int. J. Heat and Mass Transfer, vol. 44., pp. 39-53.*

Paul, B., 1962, Compilation of Evaporation Coefficients, *ARS J.*, vol. 32, no. 9, pp. 1321-1328.

Picker, G., 1998, Nicht-Gleichgewichts-Effekte beim Wachsen und Kondensieren von Dampfblasen, *Dissertation, Herbert Utz Verlag*, München, ISBN 3-89675-329-0

Pound, G. M., 1972, Selected Values of Evaporation and Condensation Coefficients for Simple Substances, *J. Phys. Chem. Ref. Data*, vol. 1, no. 1, pp. 135-146.

Plesset, M. S., and Zwick, S. A., 1954, The Growth of Vapor Bubbles in Superheated Liquid, *J. of Appl. Phys.*, vol. 25, pp. 493-500.

Schrage, R., 1953, A Theoretical Study of Interphase Mass Transfer, *Columbia*, New York.

Scriven, L. E., 1959, On the Dynamics of Phase Growth, *Chem. Eng. Sci.*, vol. 10, no. 1/2, pp. 1 - 13.

Stralen, S. van, and Cole, R., 1979, Boiling Phenomena, *Hemisphere*, Washington.